
A SIMULTANEOUS APPROACH FOR TRAINING NEURAL DIFFERENTIAL-ALGEBRAIC SYSTEMS OF EQUATIONS

A PREPRINT

Laurens R. Lueg *
llueg@andrew.cmu.edu

Victor Alves *
vcunhaal@andrew.cmu.edu

Daniel Schicksnus *,†

John R. Kitchin *
jkitchin@andrew.cmu.edu

Carl D. Laird *
claird@andrew.cmu.edu

Lorenz T. Biegler *
lb01@andrew.cmu.edu

ABSTRACT

Neural differential-algebraic systems of equations (DAEs) are a modeling paradigm where some unknown relationships within a DAE are modeled with a neural network and learned from data. Training neural DAEs is more challenging than training neural ordinary-differential equations (ODEs), particularly for higher-index systems. Existing approaches utilize differentiable pipelines, usually comprising integration, projection, operator splitting, or penalty terms for algebraic constraints. The parameters are then updated in a sequential manner using gradient descent. In this work, we employ the simultaneous approach for DAE-constrained parameter estimation instead. This defines a fully discretized nonlinear programming program (NLP), whose solution simultaneously obtains the neural network parameters and the trajectories of the corresponding DAE, while enforcing constraint satisfaction at the discretization points. We show that with careful initialization and handling of the neural network terms, this approach can be efficient for smaller-scale problems, including higher-index DAEs. As the number of parameters or the amount of data increase, decomposition strategies are necessary to make this method scalable. We present an approach which is inspired by existing sequential approaches. However, a tractable, discretized NLP is solved at every iteration of gradient descent and the sensitivity of its solution with respect to the neural network parameters is evaluated in an efficient manner. We demonstrate the scalability of this decomposition with respect to the number of parameters and the size of the training data set.

Keywords Nonlinear Programming, Neural DAEs, Dynamic Optimization, Hybrid Modeling, Differentiable Optimization

1 Introduction

The development of modeling paradigms that combine mechanistic and data-driven components has become an important task for researchers and practitioners in the area of science and engineering, promising to provide scalable computational solutions which can make use of data and incorporate first-principles-based system knowledge. Notable examples include physics-informed neural networks (PINNs) [Raissi et al., 2019], neural ordinary differential equations (neural ODEs) [Chen et al., 2018, Kidger, 2022] and universal differential equations (UDEs) [Rackauckas et al., 2020], which have been applied in various fields, such as bioprocesses [Bangi et al., 2022], crystallization [Lima et al., 2025], model-predictive control [Luo et al., 2023, Casas et al., 2025], wastewater treatment [Huang et al., 2025], battery modeling [Huang et al., 2024], power systems [Xiao et al., 2022] and parameter estimation in process systems engineering applications [Bradley and Boukouvala, 2021].

A recent extension to this field of research are so-called neural differential-algebraic systems of equations (neural DAEs), which combine neural ODEs or UDEs with algebraic constraints. Depending on the application, these con-

*Department of Chemical Engineering, Carnegie Mellon University, Pittsburgh, PA 15213.

†RWTH Aachen University, Process Systems Engineering (AVT.SVT), Aachen 52074, Germany

straints might be known or learned from data themselves. Related topics include the reconciliation of learned models with algebraic constraints [Mukherjee and Bhattacharyya, 2025], as well as the integration of learned system dynamics with optimal control [Di Vito et al., 2024]. Several works discuss the use of PINNs for DAEs [Moya and Lin, 2023, Chen et al., 2023, Luo et al., 2025]. There, the numerical solution of a (known) DAE is replaced by the evaluation of one or multiple deep neural networks, which are trained using a physics-informed loss function. This differs slightly from the training of neural DAEs, the topic of this work, which aims to approximate unknown components of a DAE using neural networks.

Training algorithms for neural DAEs usually rely on computing derivatives of a loss function with respect to the parameters of the neural network through a pipeline of computational operations, including integration to deal with the differential part of the model, as well as projection [White et al., 2024, Pal et al., 2025], operator splitting [Koch et al., 2025] and/or the use of penalty terms [Tuor et al., 2020, Neary et al., 2024, Huang et al., 2024, Xiao et al., 2022] to handle algebraic constraints. The parameters are then updated using (stochastic) gradient descent, and the pipeline is evaluated anew; we will refer to this type of approach as sequential. Sequential approaches are often computationally scalable with respect to the amount of data, as the pipeline can be evaluated in parallel for different batches, and with respect to the number of neural network parameters, in part due to the capabilities of modern automatic differentiation (AD) implementations for deep learning. Nevertheless, gradient descent often requires manual tweaking of its parameters and many iterations to converge to a satisfactory solution – for neural ODEs/DAEs each iteration can be costly [Roesch et al., 2021].

Similar observations have been made in the past about parameter estimation problems constrained by purely mechanistic DAEs, giving rise to simultaneous solution approaches: the DAE is fully discretized, using e.g. orthogonal collocation, and a nonlinear programming solver is used to solve the resulting optimization problem [Biegler, 2007]. This avoids the repeated call to a DAE/ODE routines, and makes use of powerful nonlinear programming solvers, such as IPOPT [Wächter and Biegler, 2006]. DAE-constrained optimization problems can be easily modeled in continuous time with software tools such as APMONITOR [Hedengren et al., 2014], INFINTEOPT.JL [Pulsipher et al., 2022] or PYOMO.DAE [Nicholson et al., 2018], which automatically discretize the problem and send it to a solver. Hence, in this work we investigate the use of the simultaneous approach for training neural DAEs. A similar approach has recently demonstrated promising results on small-scale neural ODEs [Shapovalova and Tsay, 2025]. For the case of DAEs, the simultaneous approach has the added advantage of being able to handle higher-index DAEs (given the use of an appropriate discretization scheme), as well as rigorously enforcing algebraic constraints, which is not guaranteed with penalty-based training methods.

The resulting nonlinear optimization problems are potentially large, depending on the size of the neural network and the number of trajectories where data are available. Furthermore, neural network expressions are dense with respect to their trainable parameters, which increases the computational cost of solving the associated optimization problems. We demonstrate that these issues can be dealt with to successfully apply the simultaneous approach to medium-scale neural DAEs. In addition, we will show that the simultaneous approach can also be leveraged to define sequential training approaches, which retain both favorable scaling properties and aforementioned advantages related to constraint satisfaction and higher-index systems.

1.1 Contributions

This work makes the following novel contributions to the field of computational optimization applied to the training neural DAEs:

- The neural DAE training problem is formulated generally and the simultaneous approach is applied. This allows for consideration of a wider range of systems than previously, including higher-index DAEs and/or systems with inequality constraints.
- A tailored solution approach for the resulting NLP is proposed, including a specialized initialization scheme for neural DAEs, the use of Hessian approximations and the evaluation of neural network expressions using external gray-box models.
- A decomposition scheme which improves the scalability of the proposed approach by leveraging efficient evaluation of NLP sensitivities with respect to neural network parameters.

1.2 Outline

In Section 2, we provide a general framework for neural DAEs and formulate the training problem which our work addresses. We then describe how the simultaneous approach is applied to this problem in Section 3, and present specific steps to make the resulting NLP more tractable. Furthermore, we discuss decomposition approaches in Section 3.3 and

introduce a sequential method which leverages the simultaneous approach and NLP sensitivities to improve scalability. We evaluate the proposed methods on several case studies in Section 4, including scalability analysis. We conclude with a discussion of the strengths and limitations of our proposed methods, and related recommendations for future work in Sec. 5.

2 Problem statement

In this work, we consider the semi-explicit neural DAE defined as

$$\frac{d\mathbf{x}}{dt} = \mathbf{f}(\mathbf{x}(t), \mathbf{y}(t), \mathbf{z}(t), \mathbf{p}), \quad \forall t \in [t_0, t_f] \quad (1a)$$

$$0 = \mathbf{h}(\mathbf{x}(t), \mathbf{y}(t), \mathbf{z}(t), \mathbf{p}), \quad \forall t \in [t_0, t_f] \quad (1b)$$

$$0 = \mathbf{z}(t) - \mathbf{f}_{\text{NN}}(\mathbf{v}(t), \boldsymbol{\theta}), \quad \mathbf{v}(t) \subseteq \{\mathbf{x}(t), \mathbf{y}(t), \mathbf{p}\} \quad \forall t \in [t_0, t_f] \quad (1c)$$

$$\mathbf{x}(t_0) = \mathbf{x}_0(\mathbf{p}), \quad (1d)$$

with differential variables $\mathbf{x}(t) \in \mathbb{R}^{n_x}$, algebraic variables $\mathbf{y}(t) \in \mathbb{R}^{n_y}$ and $\mathbf{z}(t) \in \mathbb{R}^{n_z}$, and independent static variables $\mathbf{p} \in \mathbb{R}^{n_p}$. The neural network $\mathbf{f}_{\text{NN}} : \mathbb{R}^{n_v+n_\theta} \mapsto \mathbb{R}^{n_z}$ is parametrized by $\boldsymbol{\theta} \in \mathbb{R}^{n_\theta}$ and links the unknown terms in the model, $\mathbf{z}(t)$, to a subset of the remaining variables, i. e., the inputs of the neural network, labeled $\mathbf{v}(t) \in \mathbb{R}^{n_v}$. Often, domain knowledge allows one to define a structural prior on which variables should be considered as input to the neural network. We assume that $\mathbf{f} : \mathbb{R}^{n_x+n_y+n_z+n_p} \mapsto \mathbb{R}^{n_x}$, $\mathbf{h} : \mathbb{R}^{n_x+n_y+n_z+n_p} \mapsto \mathbb{R}^{n_y}$, and \mathbf{f}_{NN} are Lipschitz continuous for $t \in [t_0, t_f]$, when \mathbf{p} and $\boldsymbol{\theta}$ are specified. The initial state of the differential variables may depend on some of the independent static variables (1d); indeed, the initial state might be unknown and thus included in \mathbf{p} . To determine the index of (1), (1c) is substituted into the other equations to obtain the algebraic constraint

$$0 = \mathbf{h}(\mathbf{x}(t), \mathbf{y}(t), \mathbf{f}_{\text{NN}}(\mathbf{x}(t), \boldsymbol{\theta}), \mathbf{p}). \quad (2)$$

For a given \mathbf{p} and $\boldsymbol{\theta}$, if $\nabla_{\mathbf{y}}\mathbf{h}$ is non-singular (for all $t \in [t_0, t_f]$), the DAE (1) is index-1. Otherwise, the index can be defined by the minimum number of differentiations of the DAE system that are necessary to obtain ODEs for the algebraic variables $\mathbf{y}(t)$. Thus, the analysis of the index of (1) is analogous to conventional DAEs [Biegler, 2010], given a particular set of parameter values \mathbf{p} and $\boldsymbol{\theta}$. At this point, we do not make specific restrictions on the index of (1). In Sec. 3, we will provide some details on how our approach can deal with higher-index DAEs.

We have access to noisy data collected from a set of trajectories (or scenarios) $\mathcal{S} = \{1, \dots, n_s\}$. Although the output terms $\mathbf{z}(t)$ of the neural network are usually unobserved, we assume that there are observations for all variables which define the input to the neural network. For the problems considered in this work, this always means the differential state variables. Thus, along each trajectory, observations of the differential states $\mathbf{x}(t)$ are available at specific times $t \in \mathcal{T}_o^s$. Observations of algebraic variables may be available as well; however, we do not consider this here.

In the remainder of this work, we will use the following notation: Vector-valued variables will be noted in lower-case bold face, with a superscript indicating the trajectory the variable is defined on, e.g. $\mathbf{x}^{(s)}(t)$. Furthermore, discretizations of continuous variables at some index k will be denoted $\mathbf{x}_k^{(s)}$. With this, we denote the observed data as:

$$\hat{\mathbf{x}}_i^{(s)} = \bar{\mathbf{x}}^{(s)}(t_i) + \boldsymbol{\epsilon}_i^{(s)}, \quad \forall s \in \mathcal{S}, \forall t_i \in \mathcal{T}_o^s,$$

where $\bar{\mathbf{x}}^{(s)}(t)$ is the *ground truth* trajectory of the underlying system. Unless otherwise stated, we expect the observation noise $\boldsymbol{\epsilon}_i^{(s)}$ to be drawn from a Gaussian distribution with mean zero. The loss incurred by a continuous state profile $\mathbf{x}^{(s)}(t)$ with respect to the observed data on trajectory s may be defined as

$$\varphi^{(s)}(\mathbf{x}^{(s)}(t)) = \sum_{t_i \in \mathcal{T}_o^s} \left\| \mathbf{x}^{(s)}(t_i) - \hat{\mathbf{x}}_i^{(s)} \right\|_2^2, \quad (3)$$

although other formulations (e.g. weighted least squares, absolute error, etc.) are possible. The general problem formulation for training the neural DAE model is then given by:

$$\min \sum_{s \in \mathcal{S}} \varphi^{(s)}(\mathbf{x}^{(s)}(t)) + \alpha_r r(\boldsymbol{\theta}) \quad (4a)$$

$$\text{s. t. } \frac{d\mathbf{x}^{(s)}}{dt} = \mathbf{f}(\mathbf{x}^{(s)}(t), \mathbf{y}^{(s)}(t), \mathbf{z}^{(s)}(t), \mathbf{p}), \quad \forall s \in \mathcal{S}, \forall t \in [t_0^s, t_f^s] \quad (4b)$$

$$\mathbf{h}(\mathbf{x}^{(s)}(t), \mathbf{y}^{(s)}(t), \mathbf{z}^{(s)}(t), \mathbf{p}) = 0, \quad \forall s \in \mathcal{S}, \forall t \in [t_0^s, t_f^s] \quad (4c)$$

$$\mathbf{g}(\mathbf{x}^{(s)}(t), \mathbf{y}^{(s)}(t), \mathbf{z}^{(s)}(t), \mathbf{p}) \leq 0, \quad \forall s \in \mathcal{S}, \forall t \in [t_0^s, t_f^s] \quad (4d)$$

$$\mathbf{z}^{(s)}(t) = \mathbf{f}_{\text{NN}}(\mathbf{x}^{(s)}(t), \boldsymbol{\theta}), \quad \forall s \in \mathcal{S}, \forall t \in [t_0^s, t_f^s] \quad (4e)$$

$$\mathbf{x}^{(s)}(t_0^s) = \mathbf{x}_0^{(s)}(\mathbf{p}), \quad \forall s \in \mathcal{S}. \quad (4f)$$

The parameters of the neural network $\boldsymbol{\theta}$ and the static parameters for the mechanistic portion of the model formulation \mathbf{p} are shared between all trajectories, while each trajectory has its own dynamic state evolution and initial conditions. A general regularization term on the weights of the neural network is included in the objective, with coefficient α_r . Unless stated otherwise, we use $r(\boldsymbol{\theta}) = \frac{1}{2} \|\boldsymbol{\theta}\|_2^2$. Note that the neural DAE (1) is embedded in the problem, under the addition of inequality, or path constraints (4d), which can represent physically-motivated variable bounds, for example. If these bounds become active, the existence of a solution to (4) might not be guaranteed unless sufficient independent variables are included in the problem. To this end, slack variables and/or barrier reformulations for (4d) may be used. Note that the above formulation is still in continuous form, i.e. the discretization of the embedded DAE has not been performed yet. As noted in Sec. 1.1, so-called sequential solution approaches transform (4) into an unconstrained optimization problem in terms of θ , where (4b)-(4f) are handled through differentiable pipelines involving integration, projection and/or penalty terms. In this work, we present the holistic solution of (4) using orthogonal collocation and nonlinear programming, i.e., the simultaneous approach for DAE-constrained optimization. Furthermore, we present a bi-level decomposition of the resulting NLP which gives rise to a scalable sequential variant of the proposed approach in Section 3.3.

3 Simultaneous approach for neural DAEs

We briefly outline the simultaneous approach before applying it to (4). At its core, this entails fully discretizing (4), transforming it into a (large-scale) nonlinear optimization problem, which can be solved using an interior point method, for example. Although this approach is agnostic to the discretization scheme, orthogonal collocation is often chosen in practice due to its favorable numerical stability and accuracy. In particular, Ascher and Petzold [1998] note that collocation methods using Radau points are well-suited for initial-value DAEs and very stiff ODEs. The application to semi-explicit index-2 DAEs usually necessitates the derivation of consistent initial conditions – as we will see, this can be directly incorporated in the nonlinear programming problem where the collocation scheme is embedded. For parameter estimation problems, potential non-uniqueness of such conditions can reasonably be expected to be resolved by the minimization of an objective function encoding data fit, if all differential states are observed. Furthermore, for higher-index problems, it has been observed that the simultaneous approach can still return solutions, albeit under some numerical strain stemming from the ill-conditioning of the underlying DAE ([Biegler, 2010], Ch. 10.4).

For the description of the collocation scheme, we omit the superscript (s) denoting the trajectory for notational brevity. The time horizon $[t_0, t_f]$ is divided into n_{fe} finite elements, where element i corresponds to the time span $[t_{i-1}, t_i]$, the length of the element is denoted by $h_i = t_i - t_{i-1}$. On each element i , the differential states $\mathbf{x}(t)$ are approximated by polynomials of degree K , $\tilde{\mathbf{x}}(t)$, using Lagrange interpolating polynomials:

$$\tilde{\mathbf{x}}(t) = \sum_{j=0}^K \ell_j(\tau) \mathbf{x}_{ij}, \quad t \in [t_{i-1}, t_i], \quad \tau \in [0, 1], \quad (5)$$

$$\text{where } t = t_{i-1} + h_i \tau \quad \text{and} \quad \ell_j(\tau) = \prod_{k=0, k \neq j}^K \frac{\tau - \tau_k}{\tau_j - \tau_k}.$$

Here, $\{\tau_j\}_{j=0, \dots, K}$ are the collocation points on each element, with $\tau_0 = 0$. The collocation points can be chosen based on different quadrature schemes, e.g. Lagrange-Radau [Biegler, 2010]. Here, we assume matching collocation points for each state in $\mathbf{x}(t)$, but this is not required. Indeed, even the number and size of the finite elements can be

adjusted specifically for each differential state. Like all aspects relating to the discretization, this would have to be specified before the resulting NLP is solved. Using the Lagrange polynomials, we have $\tilde{\mathbf{x}}(t_{i-1} + \tau_j h_i) = \mathbf{x}_{ij}$, i. e., the value of the interpolating polynomials $\tilde{\mathbf{x}}(t)$ at the collocation points is equal to the polynomial coefficients \mathbf{x}_{ij} .

After introducing similar discretizations for the algebraic variables, the continuous problem (4) is fully discretized:

$$\min \sum_{s \in \mathcal{S}} \varphi^{(s)}(\tilde{\mathbf{x}}^{(s)}(t)) + \alpha_r r(\boldsymbol{\theta}) \quad (6a)$$

$$\text{s. t. } \sum_{j=0}^K \mathbf{x}_{ij}^{(s)} \cdot \ell_j'(\tau_k) = h_i \mathbf{f}(\mathbf{x}_{ik}^{(s)}, \mathbf{y}_{ik}^{(s)}, \mathbf{z}_{ik}^{(s)}, \mathbf{p}), \quad \forall s \in \mathcal{S}, \forall i=1 \dots n_{fe}, \forall k=1 \dots K \quad (6b)$$

$$\mathbf{h}(\mathbf{x}_{ik}^{(s)}, \mathbf{y}_{ik}^{(s)}, \mathbf{z}_{ik}^{(s)}, \mathbf{p}) = 0, \quad \forall s \in \mathcal{S}, \forall i=1 \dots n_{fe}, \forall k=1 \dots K \quad (6c)$$

$$\mathbf{g}(\mathbf{x}_{ik}^{(s)}, \mathbf{y}_{ik}^{(s)}, \mathbf{z}_{ik}^{(s)}, \mathbf{p}) \leq 0, \quad \forall s \in \mathcal{S}, \forall i=1 \dots n_{fe}, \forall k=1 \dots K \quad (6d)$$

$$\mathbf{z}_{ik}^{(s)} = \mathbf{f}_{\text{NN}}(\mathbf{x}_{ik}^{(s)}, \boldsymbol{\theta}), \quad \forall s \in \mathcal{S}, \forall i=1 \dots n_{fe}, \forall k=1 \dots K \quad (6e)$$

$$\mathbf{x}_{i+1,0}^{(s)} = \sum_{j=0}^K \ell_j(1) \mathbf{x}_{ij}^{(s)}, \quad \forall s \in \mathcal{S}, \forall i=1 \dots n_{fe}, \forall k=1 \dots K \quad (6f)$$

$$\mathbf{x}_{1,0}^{(s)} = \mathbf{x}_0^{(s)}(\mathbf{p}). \quad (6g)$$

Here, the continuity of the state variables is enforced through (6f), similar constraints can be defined for the algebraic variables, if desired. Note that the continuous state profiles (the collocation polynomials) $\tilde{\mathbf{x}}^{(s)}(t)$ can be evaluated at arbitrary times in the objective, i.e., the discretization points do not have to match the points where data were observed.

We emphasize that $\mathbf{x}_{ik}, \mathbf{y}_{ik}, \mathbf{z}_{ik}, \boldsymbol{\theta}$ and \mathbf{p} are variables in Problem (6). Therefore, this problem is significantly more challenging to solve than conventional DAE-constrained optimization problems, due to the potentially large number of additional variables (the weights and biases of the neural network) and the additional constraints (6e), which are highly nonconvex and dense in $\boldsymbol{\theta}$. Solving (6) directly using a nonlinear programming solver often proved computationally intractable. Thus, in order to obtain high-quality, locally optimal solutions to (6), we apply a number of pre-processing steps, which are outlined in the following sections.

It is important to note that the formulation of the NLP (6) and its solution with an interior point method makes certain restrictions on the type of neural network we can consider. Namely, we require the function \mathbf{f}_{NN} to have smooth second-order derivatives. In this work, we will exclusively consider dense feed-forward neural networks with smooth activation functions, e.g. ‘sigmoid’, ‘softplus’, or similar. As will be discussed in Section 3.2, it is not required to be able generate algebraic expressions encoding the neural network. An interface to evaluate the function, its Jacobian, and optionally its Hessian is sufficient. Furthermore, normalization layers for the input and output of the neural network proved to aid the robustness of our approach. The associated constants can be computed from the initialization procedure outlined in Section 3.1.

3.1 Initialization strategy

In order to make the solution of (6) more tractable, we introduce an auxiliary problem, which is solved to obtain initial estimates for the trajectories of the differential states $\mathbf{x}(t)$ and algebraic variables $\mathbf{z}(t), \mathbf{y}(t)$. To this end, constraint (6e) and the variables associated with the neural network, $\boldsymbol{\theta}$, are removed from problem (6). The independent variables of this problem are the discretized unknown algebraic terms $\mathbf{z}_{ik}^{(s)}$ for each trajectory s , which are chosen to minimize the same observation loss with respect to the observed data as before, augmented with a smoothness penalty for the polynomial $\tilde{\mathbf{z}}(t)$ on each finite element:

$$\min \sum_{s \in \mathcal{S}} \left[\varphi^{(s)}(\tilde{\mathbf{x}}^{(s)}(t)) + \alpha_s \sum_{i=1}^{n_{fe}} \sum_{k,j=1}^K \|\mathbf{z}_{ij} \cdot \ell_j'(\tau_k)\|_2^2 \right] \quad (7a)$$

$$\text{s.t. } (6b), (6c), (6d), (6f), (6g) \quad (7b)$$

By solving Problem (7), we obtain trajectories for the differential and algebraic variables, which we denote by $\mathbf{x}_{\text{init}}^{(s)}(t)$ and $\mathbf{z}_{\text{init}}^{(s)}(t), \mathbf{y}_{\text{init}}^{(s)}(t)$, respectively. We also obtain values for the static variables, \mathbf{p}_{init} . They adhere to the constraints defined for the dynamic optimization problem at hand, at the discretization points defined by the collocation scheme.

Problem (7) is computationally tractable, compared to (6), as it contains fewer variables and omits the highly nonconvex constraints associated with the neural network. Furthermore, it is perfectly separable by trajectory, so the solution can be trivially parallelized. If there are static variables \mathbf{p} that must match across trajectories, their initial value can be obtained by averaging the values obtained from the solution of each subproblem.

We use the solution of (7) for three purposes related to the initialization of variables in (6). For each trajectory, we initialize $\mathbf{x}_{ik}^{(s)}$, $\mathbf{z}_{ik}^{(s)}$ and $\mathbf{y}_{ik}^{(s)}$ by evaluating $\mathbf{x}_{\text{init}}^{(s)}(t)$, $\mathbf{z}_{\text{init}}^{(s)}(t)$, and $\mathbf{y}_{\text{init}}^{(s)}(t)$ at the appropriate discretization points, respectively. Secondly, the input and output normalization layers of the neural network are fixed by computing the mean/variance of the discretized trajectories obtained from (7). Finally, we can obtain initial values for $\boldsymbol{\theta}$ by running stochastic gradient descent (SGD), with a fixed number of epochs and batch size, on a loss function defined by the trajectories for the input and output of the neural network, i.e. $\mathbf{x}_{\text{init}}^{(s)}(t)$ and $\mathbf{z}_{\text{init}}^{(s)}(t)$, respectively:

$$\varphi_{\text{init}}(\boldsymbol{\theta}) = \sum_{s \in \mathcal{S}} \sum_{t_i \in \mathcal{T}_{\text{init}}^s} \left(\mathbf{z}_{\text{init}}^{(s)}(t_i) - \mathbf{f}_{NN}(\mathbf{x}_{\text{init}}^{(s)}(t_i), \boldsymbol{\theta}) \right)^2. \quad (8)$$

The evaluation points $\mathcal{T}_{\text{init}}^s$ for this step can be chosen arbitrarily; however, it is sensible to coordinate them with the collocation scheme used to solve (6). At this point, we have obtained initial values for all relevant variables in (6), i. e., trajectories of the differential and algebraic variables, as well as the weights of the neural network. Note that the use of this initialization scheme may introduce biases towards learned representations that exhibit some degree of smoothness, which must be weighed against the potential improvements to the robustness and convergence of the solution of (6).

In the next section, we describe some of the computational challenges encountered when solving (6) using an interior point method.

3.2 Computational aspects of applying an interior point method to NLPs with neural network components

In this section, we discuss computational aspects of solving problems similar to (6), i.e., constrained, nonconvex, nonlinear optimization problems, where a subset of the variables and constraints is defined by a neural network. Since we use IPOPT throughout our approach, we follow the interior point method (IPM) as described in Wächter and Biegler [2006], highlighting the challenges arising from the incorporation of neural networks. We will omit many specifics, and refer to Wächter and Biegler [2006] for an in-depth discussion of the algorithm. Within the interior point method, a series of barrier subproblems, where inequality terms are moved to the objective, are solved while subsequently decreasing the barrier coefficient μ . For the problem (6), a general formulation of the barrier subproblem can be denoted by

$$\min_{\boldsymbol{\nu}, \boldsymbol{\theta}} f(\boldsymbol{\nu}) + \alpha_r r(\boldsymbol{\theta}) - \mu \sum_i \ln(s_i) \quad (9a)$$

$$\text{s. t. } \mathbf{c}(\boldsymbol{\nu}) = 0 \quad [\boldsymbol{\lambda}] \quad (9b)$$

$$\mathbf{d}(\boldsymbol{\nu}, \boldsymbol{\theta}) = 0 \quad [\boldsymbol{\rho}] \quad (9c)$$

$$\mathbf{g}(\boldsymbol{\nu}) + \mathbf{s} = 0 \quad [\mathbf{z}] \quad (9d)$$

where $\boldsymbol{\theta}$ are the weights and biases of the neural network, and $\boldsymbol{\nu}$ contains all other primal variables, i. e. $\boldsymbol{\nu} = (\cdots, \mathbf{x}_{ik}, \mathbf{y}_{ik}, \mathbf{z}_{ik}, \cdots, \mathbf{p})^\top$, for all discretization points ik . Slightly overloading our notation, we collect all constraints from (6) into $\mathbf{c}(\boldsymbol{\nu})$, $\mathbf{g}(\boldsymbol{\nu})$ and $\mathbf{d}(\boldsymbol{\nu}, \boldsymbol{\theta})$, where the latter contains the neural network expressions (6e). We denote the constraint multipliers in square brackets. The data fit component of the objective function is given by $f(\boldsymbol{\nu}) = \sum_{s \in \mathcal{S}} \varphi^{(s)}(\tilde{\mathbf{x}}^{(s)}(t))$. The corresponding Lagrangian is defined as

$$\mathcal{L}(\boldsymbol{\nu}, \boldsymbol{\theta}, \boldsymbol{\lambda}, \boldsymbol{\rho}, \mathbf{z}) = f(\boldsymbol{\nu}) + \alpha_r r(\boldsymbol{\theta}) - \mu \sum_i \ln(s_i) + \boldsymbol{\lambda}^\top \mathbf{c}(\boldsymbol{\nu}) + \boldsymbol{\rho}^\top \mathbf{h}(\boldsymbol{\nu}, \boldsymbol{\theta}) + \mathbf{z}^\top (\mathbf{g}(\boldsymbol{\nu}) + \mathbf{s}). \quad (10)$$

The interior-point method solves the KKT conditions of (9) using a Newton-type method. At every iteration, this produces a linear system of equations, which must be solved to obtain a step direction:

$$\underbrace{\begin{bmatrix} \mathbf{W}_{\nu\nu} + \sigma_H \mathbf{I} & \mathbf{W}_{\theta\nu}^\top & \nabla_{\nu} \mathbf{c}^\top & \nabla_{\nu} \mathbf{d}^\top & \nabla_{\nu} \mathbf{g}^\top \\ \mathbf{W}_{\theta\nu} & \mathbf{W}_{\theta\theta} + \sigma_H \mathbf{I} & 0 & \nabla_{\theta} \mathbf{d}^\top & 0 \\ \nabla_{\nu} \mathbf{c} & 0 & -\sigma_C \mathbf{I} & 0 & 0 \\ \nabla_{\nu} \mathbf{d} & \nabla_{\theta} \mathbf{d} & 0 & -\sigma_C \mathbf{I} & 0 \\ \nabla_{\nu} \mathbf{g} & 0 & 0 & 0 & -\boldsymbol{\Sigma}^{-1} \end{bmatrix}}_{\mathbf{A}} \begin{bmatrix} \mathbf{b}_{\nu} \\ \mathbf{b}_{\theta} \\ \mathbf{b}_{\lambda} \\ \mathbf{b}_{\rho} \\ \mathbf{b}_{\mathbf{z}} \end{bmatrix} = - \begin{bmatrix} \nabla_{\nu} \mathcal{L} \\ \nabla_{\theta} \mathcal{L} \\ \mathbf{c}(\boldsymbol{\nu}) \\ \mathbf{d}(\boldsymbol{\nu}, \boldsymbol{\theta}) \\ \mathbf{g}(\boldsymbol{\nu}) + \mu \mathbf{Z}^{-1} \mathbf{e} \end{bmatrix}, \quad (11)$$

where $\Sigma = \mathbf{S}^{-1} \mathbf{Z}$ and $\mathbf{e} = (1, 1, \dots, 1)^\top$. Note that δ_H and δ_C are scalar terms which are adjusted to correct the inertia of \mathbf{A} , to ensure that the resulting step direction achieves descent. The Hessian terms are given by

$$\mathbf{W}_{\nu\nu} = \nabla_{\nu\nu}^2 f(\boldsymbol{\nu}, \boldsymbol{\theta}) + \boldsymbol{\lambda}^\top \nabla_{\nu\nu}^2 \mathbf{c}(\boldsymbol{\nu}) + \boldsymbol{\rho}^\top \nabla_{\nu\nu}^2 \mathbf{d}(\boldsymbol{\nu}, \boldsymbol{\theta}) + \mathbf{z}^\top \nabla_{\nu\nu}^2 \mathbf{g}(\mathbf{x}, \boldsymbol{\theta}) \quad (12a)$$

$$\mathbf{W}_{\theta\nu} = \boldsymbol{\rho}^\top \nabla_{\theta\nu}^2 \mathbf{d}(\mathbf{x}, \boldsymbol{\theta}) \quad (12b)$$

$$\mathbf{W}_{\theta\theta} = \alpha_r \mathbf{I} + \boldsymbol{\rho}^\top \nabla_{\theta\theta}^2 \mathbf{d}(\boldsymbol{\nu}, \boldsymbol{\theta}). \quad (12c)$$

At every step of the IPM, (11) must be evaluated and solved, which poses the following computational challenges for the problem at hand:

1. Hessian and Jacobian terms involving $\boldsymbol{\theta}$, i. e., $\mathbf{W}_{\theta\nu}$, $\mathbf{W}_{\theta\theta}$ and $\nabla_{\theta} \mathbf{d}$ are dense, owing to the architecture of feed-forward neural networks. This makes them expensive to evaluate using modeling tools such as the AMPL solver library [Fourer et al., 1990], which is commonly used to generate expressions and evaluate derivatives as part of NLP solver interfaces.
2. The solution of (11) using sparse indefinite solvers such as HSL MA27 [Duff and Reid, 1982] becomes more computationally expensive, both due to the increased density and the frequent need for regularization and re-factorization stemming from the degeneracy of $\mathbf{d}(\boldsymbol{\nu}, \boldsymbol{\theta})$ in both $\boldsymbol{\nu}$ and $\boldsymbol{\theta}$.

Existing tools can be used to address the first point, namely so-called external gray-box modeling interfaces (e. g. for the PYOMO modeling language³). Thereby, the constraints involving the neural network (9c) are treated as an oracle whose value, Jacobian and Hessian can be evaluated. These evaluations can then be performed using modern deep learning toolkits such as JAX [Bradbury et al., 2018], which are specialized for these operations on neural networks. Furthermore, the specific structure of $\mathbf{d}(\boldsymbol{\nu}, \boldsymbol{\theta})$ for the problem at hand, i.e.

$$\mathbf{d}(\boldsymbol{\nu}, \boldsymbol{\theta}) = \begin{bmatrix} \vdots \\ \mathbf{z}_{ik}^{(s)} - \mathbf{f}_{\text{NN}}(\mathbf{x}_{ik}^{(s)}, \boldsymbol{\theta}) \\ \vdots \end{bmatrix}, \quad (13)$$

allows for the vectorized evaluation of the constraints and associated Jacobians/Hessians across all discretization points $\{ik\}_{\forall i=1 \dots n_f, k=1 \dots K}$ and trajectories $\{(s)\}_{\forall s \in \mathcal{S}}$ defined in (6). It should be noted that even when using this approach, the evaluation of $\mathbf{W}_{\theta\theta}$ can become expensive for large neural networks.

To sidestep this potential bottleneck and to deal with the aforementioned challenges associated with the solution of (11), an L-BFGS approximation for the Hessian terms can be used. This is a readily available option in solvers such as IPOPT and involves collecting iterate samples as the interior point method progresses to form matrices \mathbf{B} and \mathbf{M} , which define a Hessian approximation $\tilde{\mathbf{H}} = \xi \mathbf{I} + \mathbf{B} \mathbf{M} \mathbf{B}^\top$ (see Nocedal and Wright [1999], Sec. 7.2 for details). Thus, \mathbf{A} in (11) can be replaced by

$$\begin{bmatrix} \xi \mathbf{I} & 0 & \nabla_{\nu} \mathbf{c}^\top & \nabla_{\nu} \mathbf{h}^\top & \nabla_{\nu} \mathbf{g}^\top \\ 0 & \xi \mathbf{I} & 0 & \nabla_{\theta} \mathbf{h}^\top & 0 \\ \nabla_{\nu} \mathbf{c} & 0 & -\sigma_C \mathbf{I} & 0 & 0 \\ \nabla_{\nu} \mathbf{h} & \nabla_{\theta} \mathbf{h} & 0 & -\sigma_C \mathbf{I} & 0 \\ \nabla_{\nu} \mathbf{g} & 0 & 0 & 0 & -\Sigma^{-1} \end{bmatrix} + \begin{bmatrix} \mathbf{B} \\ 0 \\ 0 \\ 0 \end{bmatrix} \begin{bmatrix} \mathbf{M} \mathbf{B}^\top & 0 & 0 & 0 \end{bmatrix}. \quad (14)$$

To compute a solution to the resulting linear system, only the factorization of the left matrix in (14) is necessary (Nocedal and Wright [1999], Sec. 19.3), which is significantly cheaper than solving (11), due to increased sparsity and the fact that $\tilde{\mathbf{H}}$ is guaranteed to be positive definite, thus removing the need for curvature correction. However, because of the use of the Hessian approximation, the quality of the resulting step is often inferior, leading to an increased number of IPM iterations to converge to a solution. For the problem considered in this work (6), the use of the L-BFGS approximation proved highly effective. This is likely due to a combination of the factors described above (density, nonconvexity and Hessian evaluations). Similar results using the L-BFGS approximation were recently observed by Parker et al. [2024] when embedding trained neural networks into optimization problems. One potential drawback of the Hessian approximation strategy is that it replaces the full Hessian by an approximation. It seems more promising to only approximate the components of the Hessian which cause computational difficulties, i.e. those

³https://pyomo.readthedocs.io/en/6.4.3/contributed_packages/pynumero/pynumero.interfaces.external_grey_box_model.html

associated with the neural network. This would retain the exact Hessians of the mechanistic part of the problem thus likely improving the quality of the resulting step directions. This is an interesting avenue for future research.

In Section 4, we will show that the strategies described above, in combination with the initialization scheme from Section 3.1, make the simultaneous approach for training neural DAEs tractable for problems of small to medium scale, in terms of the size of the neural network and the number of trajectories considered. However, the approach outlined so far has a straightforward scalability issue: The size of the NLP directly scales with number of parameters in the neural network and the number of trajectories included in the training problem (6). Even when using the L-BFGS approximation and gray-box modeling components, the size and number of nonzeros in (14) increases accordingly, resulting in more costly factorizations at every step of the interior point method. Thus, to scale the approach to large-scale learning problems, decomposition approaches need to be applied.

3.3 Bi-level decomposition using NLP sensitivities

Problem (6) naturally lends itself to well-established (parallel) decomposition schemes for NLPs with block structure, where the a set of subproblems corresponding to the separate trajectories are linked by the common variables θ and \mathbf{p} (we will disregard \mathbf{p} in the following discussion in the interest of notational clarity). These kinds of structures are commonly exploited using Schur-complement approaches [Zavala et al., 2008, Kang et al., 2014] or problem-level decompositions like the alternating direction method of multipliers (ADMM) [Shapovalova and Tsay, 2025]. The latter does not guarantee convergence to a local solution for nonconvex problems, but is known to achieve good results in practice. These types of decomposition would remedy the scaling issue of the simultaneous approach for neural DAEs with respect to the number of trajectories. However, as the size of the neural network, and thereby the number of linking variables θ , grows, the parallel efficiency of Schur-complement-type decompositions is known to deteriorate [Lueg et al., 2025]. In the case of ADMM, each subproblem would still contain the linking variables, so the unfavorable scaling properties of the simultaneous approach are not expected to change.

Instead, we propose a bi-level decomposition which is conceptually similar to the sequential approaches for training neural DAEs mentioned in Section 1.1: the outer level updates the neural network parameters using (stochastic) gradient descent, where gradients are computed by evaluating the sensitivity of an inner problem, which corresponds to (6) with θ fixed. This produces much more tractable NLPs which can be trivially separated by trajectory and still benefit from the gray-box functionality to evaluate derivatives of the neural network with respect to its inputs. Furthermore, the approach leverages the initialization scheme outlined in Section 3.1, to reduce the number of gradient steps required on the outer level to converge to a satisfactory solution. Clearly, this approach will not provably converge to a locally optimal solution of (6) – however, it can ensure strict constraint satisfaction, which is of particular interest in the area of learning hybrid models. In practice, gradient descent is usually terminated once the objective stops improving significantly.

We will show that the evaluation of the sensitivity of the subproblem solutions with respect to θ can be evaluated cheaply, again leveraging software tools geared towards automatic differentiation for deep learning models.

The outer problem is defined as

$$\min_{\theta} \quad \Phi(\theta) := \alpha_r r(\theta) + \sum_{s \in \mathcal{S}} \tilde{\varphi}^{(s)}(\tilde{\mathbf{v}}^{(s)}(\theta)), \quad \text{s. t.} \quad \tilde{\mathbf{v}}^{(s)}(\theta) \in \arg \min \mathcal{S}_{\theta}^{(s)}, \quad (15)$$

where each subproblem $\mathcal{S}_{\theta}^{(s)}$ corresponds to (6) for a single trajectory s with θ fixed. For the remainder of this section, we will drop the superscript indicating the trajectory. Clearly, the subproblems can be solved in parallel and their sensitivities are summed to compute the gradient of Φ (15). With this, the subproblem is denoted as

$$\mathcal{S}_{\theta} : \quad \min_{\tilde{\mathbf{v}}, \tilde{\mathbf{s}}} \quad \tilde{\varphi}(\tilde{\mathbf{v}}) - \mu \sum_i \ln(\tilde{\mathbf{s}}_i) \quad (16a)$$

$$\text{s.t.} \quad \mathbf{c}(\tilde{\mathbf{v}}) = 0, \quad [\boldsymbol{\lambda}] \quad (16b)$$

$$\mathbf{d}_{\theta}(\tilde{\mathbf{v}}) = 0, \quad [\boldsymbol{\rho}] \quad (16c)$$

$$\tilde{\mathbf{g}}(\tilde{\mathbf{v}}) + \tilde{\mathbf{s}} = 0. \quad [\mathbf{z}] \quad (16d)$$

This is similar to the general formulation (9) introduced in Section 3, with the following adaptations:

$$\tilde{\boldsymbol{\nu}} = \begin{bmatrix} \boldsymbol{\nu}, \\ \vdots \\ \Delta_{ik}^+ \\ \Delta_{ik}^- \\ \vdots \end{bmatrix}, \quad \mathbf{d}_\theta(\tilde{\boldsymbol{\nu}}) = \begin{bmatrix} \vdots \\ \mathbf{z}_{ik} - \mathbf{f}_{\text{NN}}(\mathbf{x}_{ik}, \boldsymbol{\theta}) - \Delta_{ik}^+ + \Delta_{ik}^- \\ \vdots \end{bmatrix}, \quad \tilde{\mathbf{g}}(\tilde{\boldsymbol{\nu}}) = \begin{bmatrix} \mathbf{g}(\boldsymbol{\nu}) \\ \vdots \\ -\Delta_{ik}^+ \\ -\Delta_{ik}^- \\ \vdots \end{bmatrix}, \quad (17)$$

$$\tilde{\varphi}(\tilde{\boldsymbol{\nu}}) = \varphi(\tilde{\mathbf{x}}(t)) + \alpha \mathbf{e}^\top \sum_{ik} (\Delta_{ik}^+ + \Delta_{ik}^-). \quad (18)$$

We use the vertical dots to indicate that the constraints and variables are defined over all discretization points ik . The only significant changes are that $\boldsymbol{\theta}$ is no longer a variable and that non-negative slack variables Δ for the neural network constraints were introduced, to ensure that a feasible solution to (16) exists. The objective is modified to penalize the absolute value of these slacks – given that the coefficient α is sufficiently large, this ensures that a solution with zero slack is found, if it exists. This ensures strict constraint satisfaction as the algorithm progresses. Note that we still include the data objective in $\tilde{\varphi}$, as this proved to aid the robustness of the solution of (16).

When applying gradient descent to (15) we note that

$$\frac{d\Phi}{d\boldsymbol{\theta}} = \alpha_r \frac{dr}{d\boldsymbol{\theta}} + \nabla_{\boldsymbol{\theta}} \tilde{\boldsymbol{\nu}}(\boldsymbol{\theta})^\top \frac{d\tilde{\varphi}}{d\tilde{\boldsymbol{\nu}}}. \quad (19)$$

To compute this gradient, we need to be able to evaluate a vector product with the sensitivity of the solution of S_θ^μ with respect to $\boldsymbol{\theta}$. At the solution of (16), the KKT conditions are satisfied:

$$\mathbf{F}(\mathbf{q}(\boldsymbol{\theta}), \boldsymbol{\theta}) = \begin{bmatrix} \nabla_{\tilde{\boldsymbol{\nu}}} \tilde{\varphi} + \nabla_{\tilde{\boldsymbol{\nu}}} \mathbf{c}^\top \boldsymbol{\lambda} + \nabla_{\tilde{\boldsymbol{\nu}}} \mathbf{d}_\theta^\top \boldsymbol{\rho} + \nabla_{\tilde{\boldsymbol{\nu}}} \tilde{\mathbf{g}}^\top \mathbf{z} \\ \mathbf{c}(\tilde{\boldsymbol{\nu}}) \\ \mathbf{d}_\theta(\tilde{\boldsymbol{\nu}}) \\ \tilde{\mathbf{g}}(\tilde{\boldsymbol{\nu}}) + \tilde{\mathbf{s}} \\ \mathbf{S}\mathbf{Z} - \mu \mathbf{e} \end{bmatrix} = 0, \quad (20)$$

where $\mathbf{q}(\boldsymbol{\theta}) = (\tilde{\boldsymbol{\nu}}(\boldsymbol{\theta}), \tilde{\mathbf{s}}(\boldsymbol{\theta}), \boldsymbol{\lambda}(\boldsymbol{\theta}), \boldsymbol{\rho}(\boldsymbol{\theta}), \mathbf{z}(\boldsymbol{\theta}))^\top \in \mathbb{R}^{n_q}$ is the primal-dual solution of (16). Using the implicit function theorem, the following relation holds [Pacaud, 2025]:

$$\nabla_{\boldsymbol{\theta}} \mathbf{q}(\boldsymbol{\theta}) = -(\nabla_{\mathbf{q}} \mathbf{F}(\mathbf{q}, \boldsymbol{\theta}))^{-1} \nabla_{\boldsymbol{\theta}} \mathbf{F}(\mathbf{q}, \boldsymbol{\theta}) \quad (21)$$

$$\Rightarrow \nabla_{\boldsymbol{\theta}} \mathbf{q}(\boldsymbol{\theta})^\top \mathbf{u} = -\nabla_{\boldsymbol{\theta}} \mathbf{F}(\mathbf{q}, \boldsymbol{\theta})^\top \bar{\mathbf{u}}, \quad \text{where } \bar{\mathbf{u}} = (\nabla_{\mathbf{q}} \mathbf{F}(\mathbf{q}, \boldsymbol{\theta}))^{-\top} \mathbf{u} \in \mathbb{R}^{n_q}. \quad (22)$$

In order for the resulting sensitivities to be well-defined, we need to ensure that (16) is sufficiently regular, i.e., that linear independence constraint qualifications (LICQ) and strong second-order sufficiency conditions (SSOSC) hold. When solving (16) to local optimality using IPOPT and given that no inertia correction was necessary at the solution, these conditions are met [Pirnay et al., 2012]. Note that we solve (16) with exact Hessian information, so we can verify this at the solution of every subproblem.

To evaluate (19), we can use (22) by setting $\mathbf{u} = \left[\frac{d\tilde{\varphi}}{d\tilde{\boldsymbol{\nu}}}^\top, 0, 0, 0, 0 \right]^\top \in \mathbb{R}^{n_q}$ and similarly selecting the component corresponding to $\tilde{\boldsymbol{\nu}}$ from the resulting vector. When solving (16) using an interior point method, $\nabla_{\mathbf{q}} \mathbf{F}(\mathbf{q}, \boldsymbol{\theta})$ is the linear system factorized at every step of the algorithm – this corresponds to \mathbf{A} from (11) with the second row and column removed, since $\boldsymbol{\theta}$ is no longer a variable. A factorization of this matrix could be directly obtained from the solver at the solution, in our case we re-factorize it as we do not have direct access to the solver internals.

Evaluating $\nabla_{\boldsymbol{\theta}} \mathbf{F}(\mathbf{q}, \boldsymbol{\theta})$ can be achieved at low computational cost for problems such as (16). From (20), we have

$$\nabla_{\boldsymbol{\theta}} \mathbf{F}^\top = [\nabla_{\boldsymbol{\theta}} (\nabla_{\tilde{\boldsymbol{\nu}}} \mathbf{d}_\theta^\top \boldsymbol{\rho})^\top, 0, \nabla_{\boldsymbol{\theta}} \mathbf{d}_\theta^\top, 0, 0] \in \mathbb{R}^{n_\theta \times n_q}, \quad (23)$$

$$\Rightarrow \nabla_{\boldsymbol{\theta}} \mathbf{F}^\top \bar{\mathbf{u}} = \nabla_{\boldsymbol{\theta}} (\nabla_{\tilde{\boldsymbol{\nu}}} \mathbf{d}_\theta^\top \boldsymbol{\rho})^\top \bar{\mathbf{u}}_{\tilde{\boldsymbol{\nu}}} + \nabla_{\boldsymbol{\theta}} \mathbf{d}_\theta^\top \bar{\mathbf{u}}_\rho \in \mathbb{R}^{n_\theta}, \quad (24)$$

where we indicated particular components of $\bar{\mathbf{u}}$ by subscripts indicating the corresponding component in \mathbf{q} . Using the definition of \mathbf{d}_θ from (17), we get

$$\nabla_{\boldsymbol{\theta}} (\nabla_{\tilde{\boldsymbol{\nu}}} \mathbf{d}_\theta^\top \boldsymbol{\rho})^\top \bar{\mathbf{u}}_\nu = \sum_{ik} -\nabla_{\boldsymbol{\theta}} (\nabla_x \mathbf{f}_{\text{NN}}(\mathbf{x}_{ik}, \boldsymbol{\theta})^\top \boldsymbol{\rho}_{ik})^\top \bar{\mathbf{u}}_{x_{ik}}, \quad (25)$$

$$\nabla_{\boldsymbol{\theta}} \mathbf{d}_\theta^\top \bar{\mathbf{u}}_\rho = \sum_{ik} -\nabla_{\boldsymbol{\theta}} \mathbf{f}_{\text{NN}}(\mathbf{x}_{ik}, \boldsymbol{\theta})^\top \bar{\mathbf{u}}_{\rho_{ik}}. \quad (26)$$

Here, ρ_{ik} indicates the multiplier of constraint (16c) at discretization point ik . Note that the evaluation of the full vector-Jacobian product (VJP) (24) can be achieved by parallel (across discretization points ik) evaluations of VJPs of the neural network. This can be implemented with powerful automatic differentiation packages for neural networks, e.g. JAX. In (25) there are nested VJPs, however the inner evaluation only involves low-dimensional cotangent vectors (output dimension of the neural network).

Hence, the evaluation of the sensitivities is expected to be significantly cheaper than the solution of (16), which likely incurs the majority of the computational cost for each iteration of gradient descent. However, the solution time of (16) is not expected to increase significantly with larger neural networks, as they are contained in a gray-box model whose derivatives can be evaluated cheaply. The changes to the subproblems between iterations of gradient descent are expected to be minor, given appropriate outer step sizes, thus effective warm-starting can be implemented. Lastly, the subproblems corresponding to a particular (groups of) trajectories can be solved in parallel, given appropriate computing infrastructure. In this case, this means distributing the subproblems among the available central processing units (CPU), and ensuring the availability of sufficient memory to run IPOPT on each parallel rank.

4 Computational experiments

The following case studies analyze some of the capabilities of our proposed methods for different problems of the type described by (4). This includes the training procedure, as well as the performance of the trained models on inference tasks. The topic of inference merits some additional discussion here. Once a training procedure is completed, the learned relationship \mathbf{f}_{NN} or the entire neural DAE can be used for downstream tasks such as simulation, control or other optimization tasks. In our experiments, we will evaluate the accuracy of the learned neural DAE on unseen trajectories (i. e., initial conditions) of the same system. As we have access to the ground truth models, accuracy can be evaluated on the full (state) trajectory of the neural DAE. The accuracy of the learned component can also be evaluated by directly comparing it to the ground truth relationship it was meant to learn, without solving the DAE.

In this work, we have outlined two basic approaches to training neural DAEs using the simultaneous approach: the solution of a ‘fully’ simultaneous NLP (6), where the neural network parameters are directly embedded as variables, and the bi-level decomposition approach from Section 3.3, where a series of more tractable NLPs are solved while updating the neural network parameters using gradient descent. The initialization of both approaches can be refined by leveraging a smooth initialization problem, optionally in combination with the pretraining of the neural network, as outlined in Section 3.1.

We begin by quantifying the contribution that the initialization schemes and Hessian approximation make towards the tractability and accuracy of the fully simultaneous training procedure in Section 4.1.1. Then, we will investigate the scalability of both methods with respect to the size of the neural networks and the amount of training data in Sections 4.1.2-4.1.3. Lastly, we demonstrate some of the advantages of the simultaneous approach for training (cf. Section 4.2) and inference (cf. Section 4.3) for hybrid dynamic models with physically motivated (inequality) constraints.

The experiments were run on a conventional laptop, equipped with a 12th Gen Intel(R) Core(TM) i7-12700H (14 cores) and 32 GB of RAM. Scalability tests were performed on the Pittsburgh Supercomputing Center Bridges-2 system [Brown et al., 2021], using a single node equipped with two AMD EPYC 7742 CPUs, each with 64 cores, and 256 GB of RAM. The code used to generate the results shown here is made available on GitHub⁴.

4.1 Tank-manifold system

We adapt an example DAE system from Koch et al. [2024], which describes the dynamics of a closed system of four connected tanks. The differential states x_0, \dots, x_3 describe the fluid heights in the different tanks, the algebraic variables y_0, \dots, y_4 denote the flow rate of liquid between tanks. A pump sets the flow rate y_0 as a function of fluid heights x_0 and x_3 . The system is illustrated in Fig. 1. Importantly, the flow in y_2 is reversible, and the fluid heights x_0 and x_1 are

⁴<https://github.com/llueg/SiNDAE>

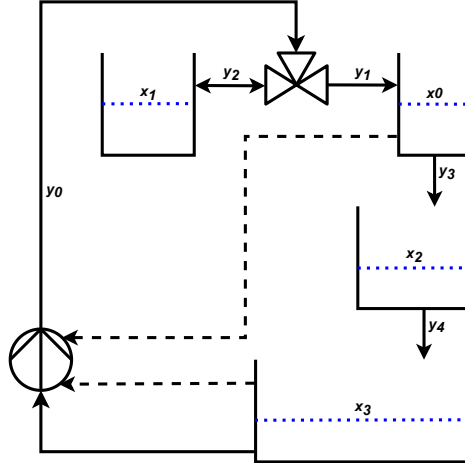


Figure 1: Tank-Manifold system adapted from Koch et al. [2024].

constrained to be equal at all times. The differential-algebraic equations describing the system are given below:

$$\frac{dx_0}{dt} = \frac{1}{\phi_0(x_0)} (y_1 - y_3), \quad (27a)$$

$$\frac{dx_1}{dt} = \frac{1}{\phi_1(x_1)} y_2, \quad (27b)$$

$$\frac{dx_2}{dt} = \frac{1}{\phi_2(x_2)} (y_3 - y_4), \quad (27c)$$

$$\frac{dx_3}{dt} = \frac{1}{\phi_3(x_3)} (y_4 - y_0), \quad (27d)$$

$$x_0(t) = x_1(t), \quad y_0(t) = y_1(t) + y_2(t), \quad y_4(t) = \frac{1}{10} \sqrt{x_2(t)} \quad (27e)$$

$$y_0(t) = \frac{1}{5} x_0 x_3, \quad y_3(t) = \frac{1}{10} \sqrt{x_0(t)}, \quad (27f)$$

$$y_0(t), y_1(t), y_3(t), y_4(t) \geq 0, \quad (27g)$$

which is an index-2 DAE. Here, $\phi_i(x_i)$ describes the area-height profile of the tanks, which is defined by their shape. We set $\phi_0(x_0)=1/10$, $\phi_1(x_1)=1/2$, $\phi_2(x_2)=2$, $\phi_3(x_3)=10$, i. e., all tanks have a constant area profiles, as is the case for cylinders, for example. However, the area of the different tanks varies. To test the methods proposed in this work, we assume no knowledge of (27f) and define the unknown terms as $\mathbf{z}(t)=(y_0(t), y_3(t))^T$. We aim to learn a neural mapping $\mathbf{f}_{NN} : \mathbf{x}(t) \mapsto \mathbf{z}(t)$. For this, we have access to noisy observations of the differential states from a given number of trajectories with different initial conditions.

4.1.1 Ablation study for ‘fully’ simultaneous approach

We investigate the importance of our proposed initialization and Hessian approximation on a small-scale training problem, where we have access to observations from three trajectories. We train our neural DAE with a neural network with two hidden layers with 30 neurons each, using the tanh activation function. There are three steps to the fully simultaneous method: trajectory initialization using (7), weight initialization (8), and solution of (6), either using L-BFGS or exact Hessian information. We are interested in the overall training time when conducting only a subset of these steps, as well as the solution that the different configurations converge to. We define five different configurations (Trials A-E, cf. Table 1). We repeated the analysis on three different training problems, where different random noise on the observations and random initialization of the NN weights (before (8) was applied, if applicable) was used, and we report the average.

For each step, we report wall-clock time. The mean-squared error (MSE) reported for training refers to the difference between the trajectories of the learned terms compared to ground truth – this gives the most direct measure of the accuracy of the learned model. From Table 1, it appears that for the problem under consideration, not using any

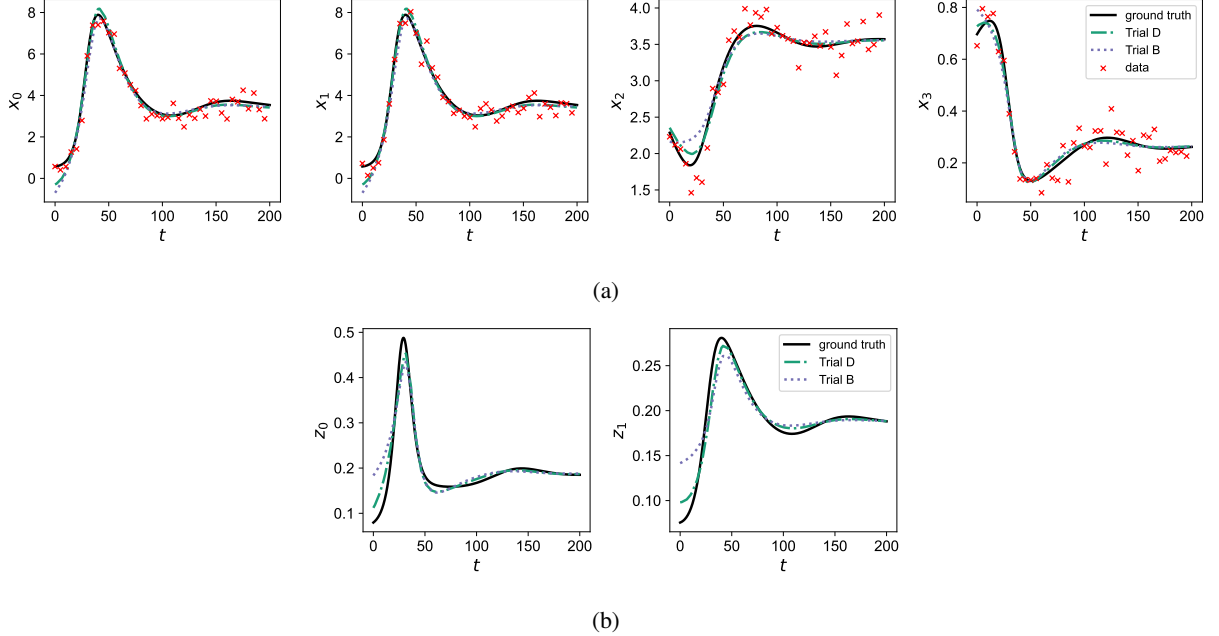


Figure 2: Comparison of trained hybrid models for different configurations from Table 1. Observed state trajectories (2a) and trajectories of the unknown terms (2b).

Table 1: Comparison of different configurations for the fully simultaneous approach

Trial	Step					Result	
	Trajectory init. (7) (s)	Weight init. (8) (s)	NLP (6), L-BFGS (s)/#iter.	NLP (6), Exact (s)/#iter.	Total (s)	MSE (train)	#Solved
A	0.260	11.300	-	202.400/51	213.900	0.087	3/3
B	0.210	10.800	25.900/108	-	36.910	0.084	3/3
C	-	-	-	711.000/180	711.000	0.067	3/3
D	-	-	32.200/134	-	32.200	0.072	2/3
E	0.220	-	27.700/119	-	27.920	0.086	3/3

initialization scheme and using exact Hessian lead to the most accurate model, however at an unacceptable computational cost (trial C). Simply switching to L-BFGS approximation reduces the solution time substantially, although this proves to be less robust, as one problem could not be solved (trial D). Using the trajectory and/or weight initialization schemes resulted in less accurate models (trials A, B, E). For the problem considered here, the bias towards smooth output trajectory proves to be significant. This is confirmed in Figure 2, where we show the fit of the models trained with configurations D (no initialization) and B (weight and trajectory initialization) on a particular trajectory in the training set. Nevertheless, the initialization schemes are effective in reducing the number of required IPM iterations, as well as the robustness of the algorithm. The weight initialization only has minor effects on the result of the training procedure.

Note that there are several hyperparameters of our approach (weight regularization, smoothing penalty coefficient, discretization scheme), which affect the specific result from the study conducted here. The authors believe the results shown here to be representative for the problem at hand.

4.1.2 Scalability of decomposition approach

In order to test whether the bi-level decomposition approach (cf. Section 3.3) is viable, two aspects are of importance: the scalability in terms of the problem size and the ability to converge to a ‘good’ solution. As opposed to the fully simultaneous approach, where termination criteria within IPOPT are well defined, there is no obvious stopping point

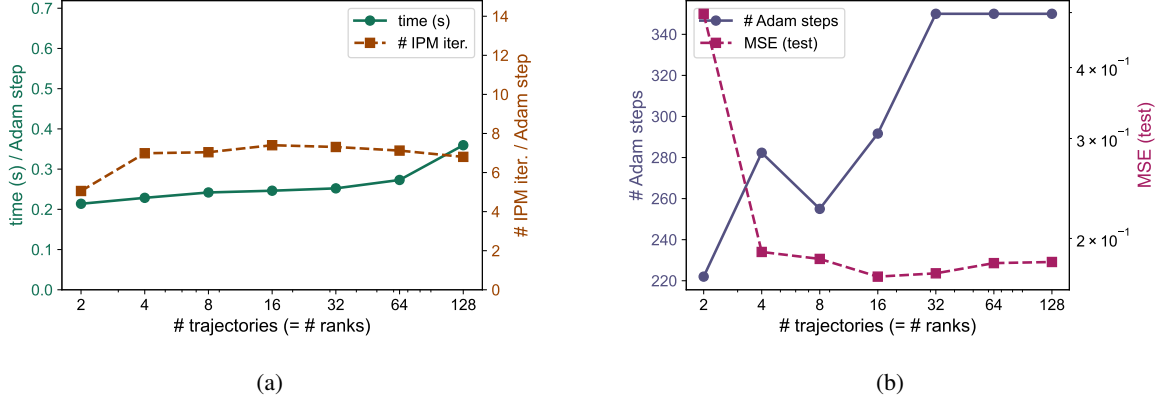


Figure 3: Scalability of bi-level decomposition with increasing amount of training data.

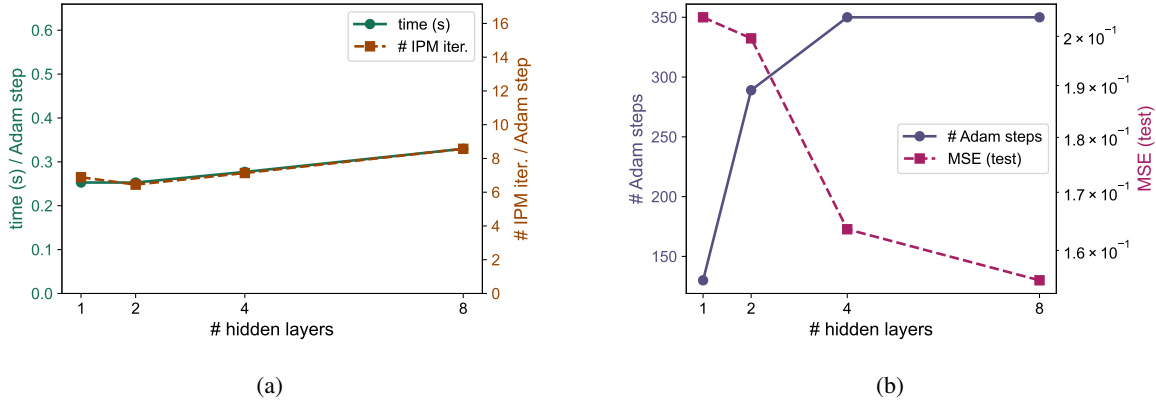


Figure 4: Scalability of bi-level decomposition with increasing size of the neural network.

for gradient descent methods, which is used to find an approximate solution to (15). In this work, we used heuristic stopping criteria which are common in the machine learning community. Namely, we systematically lower the step length, or learning rate, of the gradient descent method and terminate once no further improvement in the objective is observed, or some maximum number of steps is reached. Furthermore, we use the popular Adam optimizer [Kingma and Ba, 2014] instead of vanilla gradient descent. All results shown in this section are averaged over three executions with varying realization of noise in the observed data and weight initialization.

We begin by testing the parallel scaling of the decomposition approach with respect to the number of trajectories (cf. Figure 3), where the size of the neural network is kept constant at three hidden layers with 50 neurons each. In Figure 3a, we show that the time required per subproblem solution, as well as the associated number of IPM steps, does not change significantly as we increase the number of trajectories and ranks. This is expected, as the size of the subproblems does not change. When using all available processors on the node (128), there is a slight increase in solution time, most likely due to memory limitations. In Figure 3b, we show the number of Adam steps taken towards the solution of the upper problem (15), as well as the test set accuracy of the learned component compared to ground truth. Again, these values are tracked as the number of trajectories is increased. Evidently, for fewer trajectories the gradient descent reaches its stopping criteria before reaching the pre-defined maximum number of steps (350). The resulting models have relatively poor generalization accuracy, which is expected for small training datasets. As the size of the problem is increased, the gradient descent algorithm requires more steps and eventually reaches the upper limit. It appears that algorithmically, the gradient descent method is likely to require more iterations as the amount of data is increased, which clearly impacts the overall runtime. Tuning the learning rate and stopping criteria could improve the performance on larger data sets.

In addition, we investigate how the size of the neural network affects the performance of the decomposition scheme. For this we defined networks with 50 neurons per hidden layer and subsequently increase the number of layers. As before, we track elapsed time and IPM iterations per gradient step, total number of gradient descent steps and the

accuracy of the trained models. The size of the data set is kept constant at 50 trajectories, while using 50 parallel cores. The results are shown in Figure 4. It appears that the time required per subproblem solution does not change significantly with the size of the neural network (cf. Figure 4a). This is one of the intended advantages of the decomposition, as the neural network parameters are fixed for each subproblem solution. As before, we see that the number of Adam steps increases with increasing problem complexity (cf. Figure 4b). Furthermore, larger neural networks result in improved test accuracy of the learned models.

4.1.3 Scalability of fully simultaneous approach

We perform similar scalability tests for the fully simultaneous approach. It has to be noted that this method was not able to scale to the problem sizes considered in Section 4.1.2, as it is not parallelized and memory limitations were observed when attempting to apply the method to the training of larger neural networks, even when employing the gray-box formulation for the neural network components. Hence we repeat the analysis from Section 4.1.2 on a smaller scale. We solely focus on the solution time of the NLP (6), as the initialization steps are negligible in terms of the overall training time. We use the L-BFGS approximation for all tests in this section.

To test the scalability with respect to the number of trajectories, we used a neural network with two layers and ten neurons each. The training problem was then solved while increasing the number of included trajectories from two to 16. The time required to solve the training problem using IPOPT, as well as the number of iterations are shown in Figure 5a. As expected, the overall solution time increases significantly, as does the number of iterations. A significant portion of the solution time is spent evaluating functions and derivatives required for the KKT system at every step, which includes the evaluation of the neural network component. It appears that the vectorization across evaluation points using the gray-box model does not result in the expected insensitivity in evaluation time with respect to the number of those points.

For the same experimental setup, we compare the total time required for training and the test set accuracy of the resulting models between the fully simultaneous and decomposition approaches (cf. Figure 5b). As expected, the solution time of the simultaneous approach quickly surpasses that required for the decomposition, as the number of trajectories increases. However, the accuracy of the models trained using the simultaneous approach is significantly higher, even when compared to the larger models produced by the decomposition approach on larger training sets in Section 4.1.2. This points towards the fact that (a) the gradient descent configuration for the decomposition might be significantly tuned (b) for the problem considered here, there might not be much value in more training data, as also indicated by Figure 3b. Nevertheless, the ability of the fully simultaneous approach to find high-quality local solutions for small training problems is worth noting.

Lastly, we evaluate scalability of the fully simultaneous approach when increasing the number of layers in the trained model (cf. Figure 5c), where the number of neurons per layer is fixed at ten. Here, we only consider two trajectories for each problem. Interestingly, the number of iterations required by the solver does not increase significantly with more layers, although the overall solution time still does. This means that the time per iteration increases significantly. In combination with the relatively low portion of time spent in function evaluations, this points towards the fact that the factorization of the linear system at every step becomes more costly as the size of the neural network is increased. This is plausible as the sparsity of the system decreases for larger neural networks, which negatively impacts the performance of the linear solver.

4.2 Population dynamics

The following ODE describes the dynamics of a general predator-prey system, and is frequently used as a baseline to analyze population dynamics [Bazykin, 1998]:

$$\frac{dx_0}{dt} = (r_1 - a_1x_1 - b_1x_0)x_0, \quad (28a)$$

$$\frac{dx_1}{dt} = (r_2 - a_2\frac{x_1}{x_0})x_1, \quad (28b)$$

where $x_0(t)$ and $x_1(t)$ describe the population of the prey and predator, respectively. The constant, positive parameters $a_1=1/5, a_2 = 1/100, r_1=1/5, r_2=1/5, b_1=1/10$ describe the behavior of the populations. As a test case for our hybrid model, we assume that the term $z(t)=r_2 - a_2\frac{x_1}{x_0}$ in (28b) is unknown and apply the approach described in Sec. 3 to find a mapping $\mathbf{f}_{NN} : \mathbf{x}(t) \mapsto z(t)$. Furthermore, we assume knowledge of the following Lyapunov function for (28) [Korobeinikov, 2001]:

$$V = \ln\left(\frac{x_0}{x_0^*}\right) + \frac{x_0^*}{x_0} + \frac{a_1x_0^*}{a_2} \left(\ln\left(\frac{x_1}{x_1^*}\right) + \frac{x_1^*}{x_1} \right), \quad (29)$$

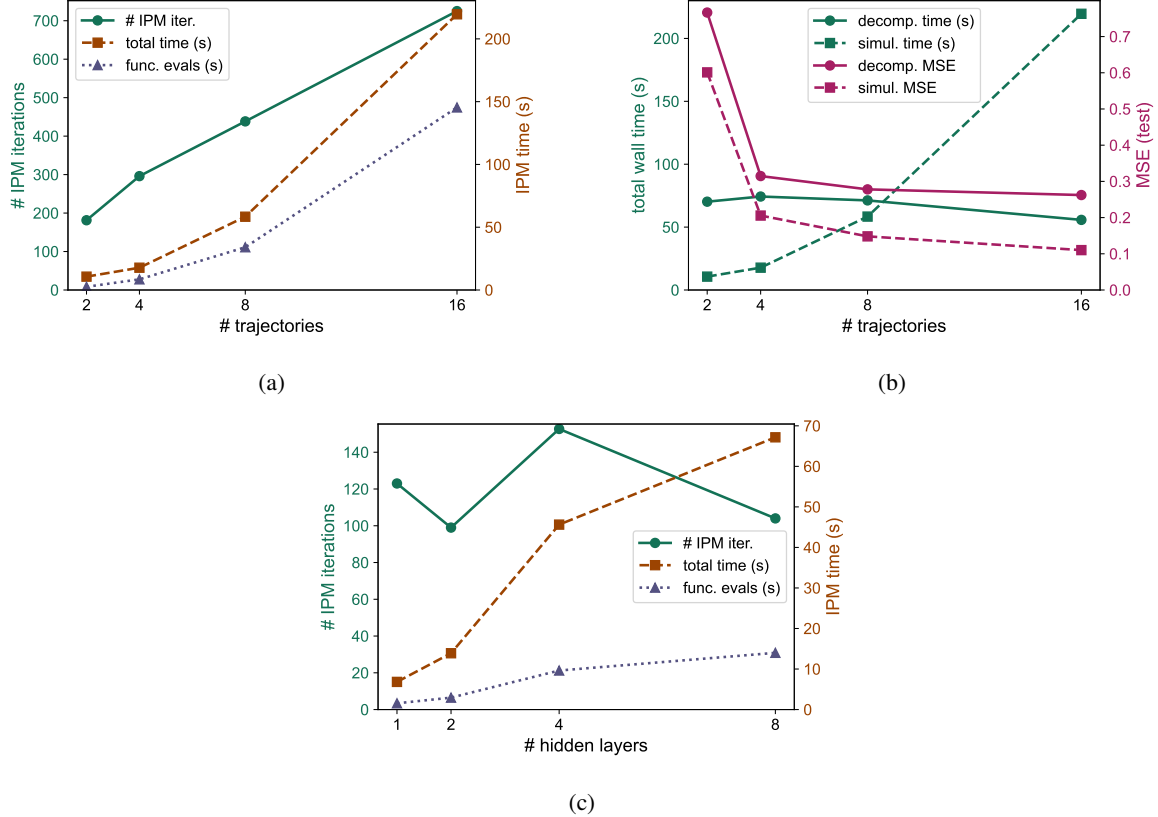


Figure 5: Scalability of the fully simultaneous approach when increasing the number of trajectories (a). Comparison of total runtime and model accuracy for the simultaneous and decomposition approach (b). Scalability of the fully simultaneous approach when increasing the size of the trained model (c).

where $x_0^* = \frac{r_1 a_2}{a_1 r_2 + a_2 b_1}$ and $x_1^* = \frac{r_1 r_2}{a_1 r_2 + a_2 b_1}$ denote the fixed point of the system. We use this to define $V(t)$ as a differential variable in the training problem and impose a path constraint $\frac{dV}{dt} \leq 0$. This enforces the state trajectories learned by our method to adhere to the Lyapunov function, which is expected to yield learned mappings that generalize better.

4.2.1 Effect of smoothing penalty

In Fig. 6, we illustrate how the solutions of the smooth initialization problem (7) are affected by the choice of smoothing coefficient α_s . For a single observed trajectory, we plot the resulting trajectories for the states and unknown terms. Note that the neural map for the unknown terms has not been included into the problem formulation at this point. It is evident that a low smoothing coefficient results in jagged trajectories, whereas increasing it produces smooth trajectories which fit the observations less accurately.

4.2.2 Effect of Lyapunov-based path constraints

We now demonstrate how including physically-motivated path constraints, such as the enforcing the descent of the Lyapunov function in (28), can significantly improve a learned hybrid model, especially in cases where little data are available. In Fig. 7b, the trajectories of two models fitted with our approach are plotted, one with and one without the path constraint. Including the constraint leads to a model which has much improved generalization capabilities, as shown by the phase plot produced by the two learned models in Fig. 7d. Without including the constraint, the descent property of the learned model is clearly violated (7c). This example is perhaps slightly contrived, as knowing the Lyapunov function is unlikely in cases where the system dynamics themselves are not fully known. However, this case study succinctly demonstrates the flexibility of the simultaneous approach in dealing with non-trivial constraints. In this example, we used a neural network with two hidden layers, each with 10 neurons using the tanh activation function.

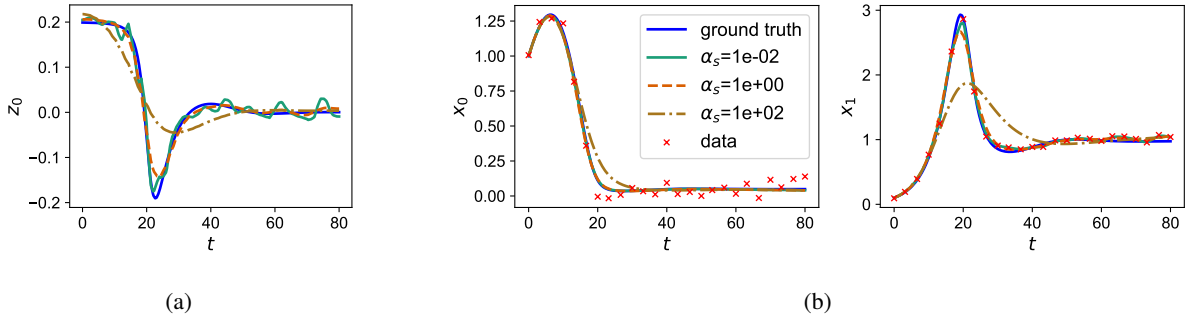


Figure 6: Smoothed trajectory of unknown term $z(t)$ (a), and states $x(t)$ (b), for varying smoothing penalties α_s . The observations are shown in red.

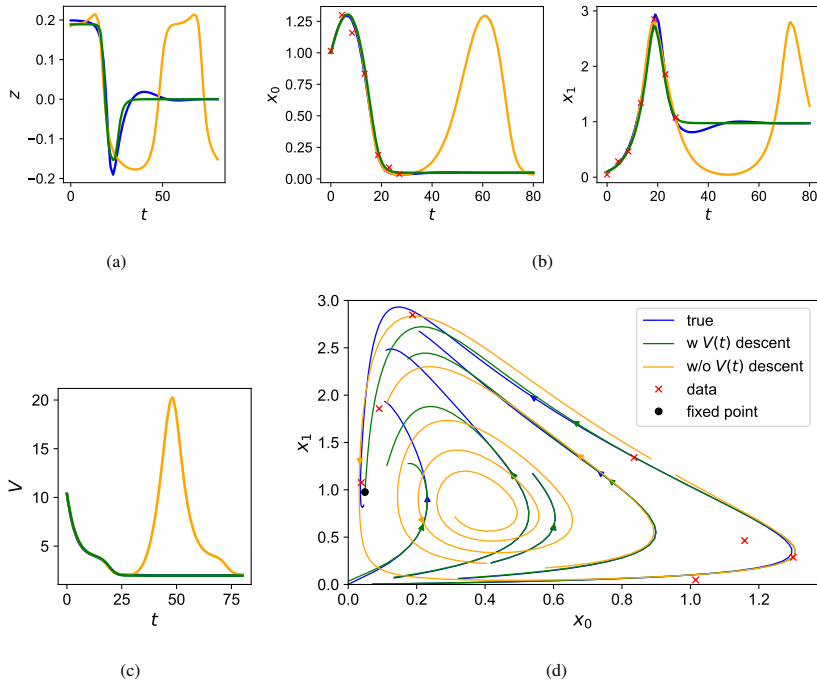


Figure 7: State trajectory of the hybrid systems, which are learned with and without the path constraint enforcing Lyapunov descent (7b). Including the constraints leads to a more accurate model, especially beyond the point where data are observed. The output of the neural map (7a) shows similar improvement when compared with the true model.

4.3 Fed-batch bioreactor

We consider a model of a fed-batch bioreactor, adapted from Kantor [2021]. In this system, a generic cell bioproduct is generated, which is a relevant case study in the area of bio-pharmaceutics. The ODEs for cell concentration X [g/L], desired product concentration P [g/L], necessary substrate concentration S [g/L], and volume V [L/h] are given by:

$$\frac{dX}{dt} = -\frac{F(t)}{V(t)} \cdot X(t) + \mu(S(t)) \cdot X(t) \quad (30a)$$

$$\frac{dP}{dt} = -\frac{F(t)}{V(t)} \cdot P(t) + Y_{P/X} \cdot \mu(S(t)) \cdot X(t) \quad (30b)$$

$$\frac{dS}{dt} = \frac{F(t)}{V(t)} \cdot (S_f - S(t)) - \frac{1}{Y_{X/S}} \cdot \mu(S(t)) \cdot X(t) \quad (30c)$$

$$\frac{dV}{dt} = F(t) \quad (30d)$$

$$X(t), P(t), S(t), V(t) \geq 0, \quad \forall t \in [t_0, t_f] \quad (30e)$$

where $F(t)$ [L/h] corresponds to a feed profile that maintains the substrate at a viable concentration for the cell growth. For a Monod-type kinetic model, we have

$$\mu(S(t)) = \mu_{\max} \frac{S(t)}{K_S + S(t)}, \quad (31)$$

where μ_{\max} [h^{-1}] is maximum specific growth rate and K_S [$\frac{g}{L}$] the half-saturation kinetic constant. Other parameters of the system include the feed substrate concentration $S_f = S(t_0)$, the yield coefficient for new cells $Y_{X/S}$ and the product yield coefficient, $Y_{P/X}$. We adopt these parameters (except the initial state) from [Kantor, 2021].

In this example, we seek to learn a relationship $f_{\text{NN}} : (X, P, S, V) \mapsto \mu$ from observations of the state variables, i. e., we assume no knowledge of (31). For this example, we wish to focus on the inference task. Once f_{NN} is trained, it can be embedded into (30), and the resulting ODE can be evaluated on new initial conditions. However, when using an integrator directly, the resulting trajectories are not guaranteed to obey physical limits, such as the lower bounds on the state variables (30e). This applies regardless of which method was used to train f_{NN} , although there might be differences in the frequency at which such bounds are violated. Alternatively, the simultaneous neural DAE framework described in this work can also be used for inference tasks. For the system at hand, the following NLP is formulated and discretized using the approach outlined in Section 3:

$$\min \int_{t_0}^{t_f} |\Delta^+(t) + \Delta^-(t)| dt \quad (32a)$$

$$\text{s. t. } \frac{dX}{dt} = -\frac{F(t)}{V(t)} \cdot X(t) + z(t) \cdot X(t) \quad (32b)$$

$$\frac{dP}{dt} = -\frac{F(t)}{V(t)} P(t) + Y_{P/X} \cdot z(t) \cdot X(t) \quad (32c)$$

$$\frac{dS}{dt} = \frac{F(t)}{V(t)} \cdot (S_f - S(t)) - \frac{z(t)}{Y_{X/S}} \cdot X(t) \quad (32d)$$

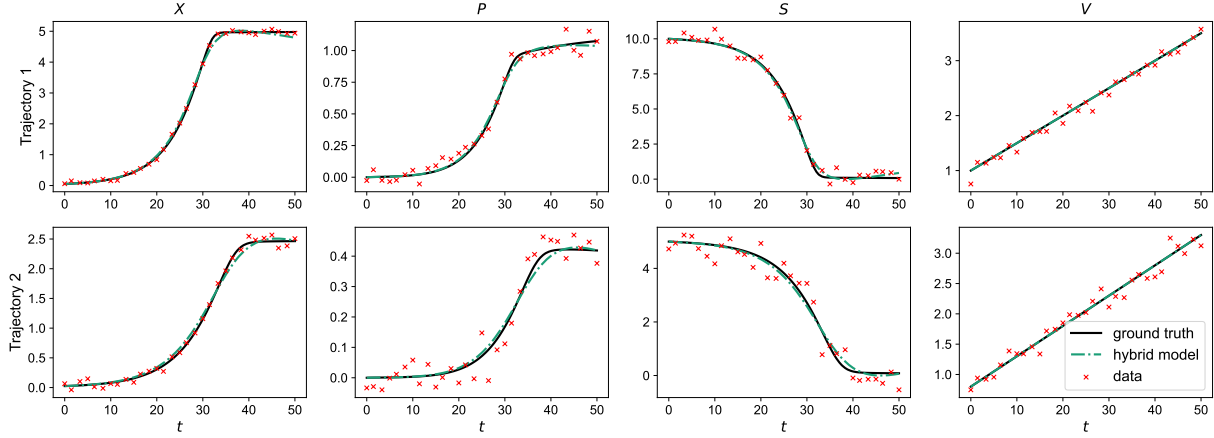
$$\frac{dV}{dt} = F(t) \quad (32e)$$

$$z(t) = f_{\text{NN}}(X(t), P(t), S(t), V(t), \boldsymbol{\theta}) + \Delta^+(t) - \Delta^-(t) \quad (32f)$$

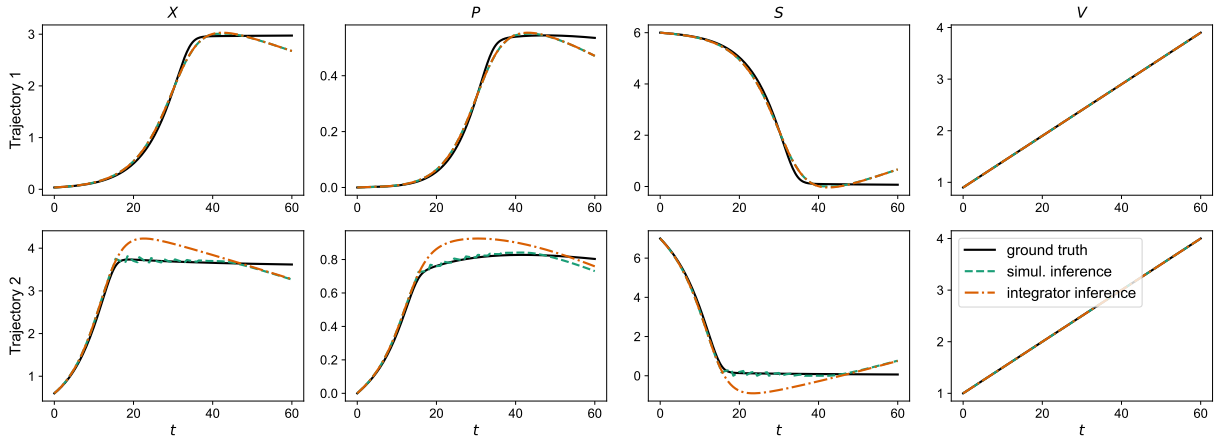
$$X(t), P(t), S(t), V(t), \Delta^+(t), \Delta^-(t) \geq 0, \quad \forall t \in [t_0, t_f]. \quad (32g)$$

Note that for inference, $\boldsymbol{\theta}$ is fixed. Furthermore, we have added slack variables to the constraint defining the learned relationship. This allows the solution of (32) to obey other constraints defined in the system, e.g. lower bounds on the state variables by modulating the output of the trained neural network when necessary.

To illustrate this, a hybrid model was trained using the fully simultaneous approach in Section 3, although any of the other approaches can be applied as well. The model was trained on only two trajectories, where it achieved a good fit (cf. Figure 8a). Due to few training data, the trained model is not likely to generalize well. In Figure 8b, we evaluate the trained hybrid ODE on two unseen initial conditions. We use both a standard integrator (Runge-Kutta 45 from SCIPY [Virtanen et al., 2020]) and the simultaneous approach (32) to compute the trajectories for the learned model.



(a)



(b)

Figure 8: A hybrid model is trained on two trajectories (a) and evaluated on two new initial conditions (b). Performing inference using the simultaneous approach ensures known constraints (here, $S(t) \geq 0$) are respected.

The results show that the trajectories produced by the two approaches agree, when none of the constraints would be violated (Trajectory 1 in Figure 8b). However, the simultaneous inference approach ensures the satisfaction of bound constraints, even where the straightforward integration of the learned model does not (Trajectory 2 in Figure 8b), and thereby produces a trajectory closer to ground truth, in this example. For simple problems like the one considered here, integration schemes can be modified to achieve similar effects. However, for the larger class of DAEs, it is usually less straight-forward to obey algebraic constraints. The evaluation of the inference scheme outlined here on a wider range of problems appears to be an interesting area for further research.

5 Conclusion

In this work, we investigate the applicability of the simultaneous approach for dynamic optimization to the training of so-called neural differential-algebraic systems of equations (neural DAEs). We adopt a modeling framework for neural DAEs which focuses on hybrid models, i. e. systems where only a subset of the differential or algebraic equations is approximated with a neural network, which is trained on observed data. We formulate the training task as a DAE-constrained optimization problem, and propose the use of the simultaneous approach to produce a discretized nonlinear programming problem (NLP), which is solved using an NLP solver, such as IPOPT. To improve the tractability of the resulting NLP, we devise a specialized initialization scheme, as well as the use of existing solver and modeling configurations, namely L-BFGS Hessian approximations and gray-box models, respectively.

Furthermore, we propose a bi-level decomposition approach to tackle the scalability issues of the simultaneous approach with respect to the size of the neural network and the amount of training data. On the lower level, this leverages implicit differentiation of the solutions of the subproblems with respect to the neural network parameters, which are updated on the upper level using a gradient descent method.

In our computational experiments, we demonstrate that the simultaneous approach can effectively solve training problems of small to moderate sizes, including on higher-index DAE systems. In a scalability study, it is shown that the decomposition approach is able to scale to much larger problems through the parallel evaluation of subproblems and the separation of the neural network parameters from the solution of the NLPs. As is typical with first-order gradient-based training methods, hyperparameters and stopping criteria need to be chosen, which often requires problem-specific tuning. In fact, the fully simultaneous approach is shown to converge to better solutions than the sequential bi-level decomposition on small training problems.

Finally, there are several important avenues for future research and improvements. The efficacy of the methods proposed here should be evaluated on a wider range of systems, potentially including data from real experimental testbeds to assess the value of DAE-based hybrid models. The applicability of the simultaneous approach to inference tasks involving neural DAEs could also be studied in more detail. Furthermore, the implementation of the decomposition approach could be improved by integrating the NLP solver and implicit differentiation more closely, e. g. by making use of existing tools to evaluate sensitivity in IPOPT [Biegler and Thierry, 2018, Pirnay et al., 2012]. Furthermore, automatic differentiation and NLP solution could be conducted on graphical processing units to scale to larger learning tasks – this has been an active area of development in recent years [Parker et al., 2025].

References

- M. Raissi, P. Perdikaris, and G.E. Karniadakis. Physics-informed neural networks: A deep learning framework for solving forward and inverse problems involving nonlinear partial differential equations. *Journal of Computational Physics*, 378:686–707, 2019. ISSN 0021-9991. doi: <https://doi.org/10.1016/j.jcp.2018.10.045>. URL <https://www.sciencedirect.com/science/article/pii/S0021999118307125>.
- Ricky TQ Chen, Yulia Rubanova, Jesse Bettencourt, and David K Duvenaud. Neural ordinary differential equations. *Advances in neural information processing systems*, 31, 2018.
- Patrick Kidger. On neural differential equations. *arXiv preprint arXiv:2202.02435*, 2022.
- Christopher Rackauckas, Yingbo Ma, Julius Martensen, Collin Warner, Kirill Zubov, Rohit Supekar, Dominic Skinner, Ali Ramadhan, and Alan Edelman. Universal differential equations for scientific machine learning. *arXiv preprint arXiv:2001.04385*, 2020.
- Mohammed Saad Faizan Bangi, Katy Kao, and Joseph Sang-II Kwon. Physics-informed neural networks for hybrid modeling of lab-scale batch fermentation for β -carotene production using *saccharomyces cerevisiae*. *Chemical Engineering Research and Design*, 179:415–423, 2022. ISSN 0263-8762. doi: <https://doi.org/10.1016/j.cherd.2022.01.041>. URL <https://www.sciencedirect.com/science/article/pii/S0263876222000491>.
- Fernando Arrais R.D. Lima, Marcellus G.F. de Moraes, Amaro G. Barreto, Argimiro R. Secchi, Martha A. Grover, and Maurício B. de Souza. Applications of machine learning for modeling and advanced control of crystallization processes: Developments and perspectives. *Digital Chemical Engineering*, 14:100208, 2025. ISSN 2772-5081. doi: <https://doi.org/10.1016/j.dche.2024.100208>. URL <https://www.sciencedirect.com/science/article/pii/S277250812400070X>.
- Junwei Luo, Fahim Abdullah, and Panagiotis D. Christofides. Model predictive control of nonlinear processes using neural ordinary differential equation models. *Computers & Chemical Engineering*, 178:108367, 2023. ISSN 0098-1354. doi: <https://doi.org/10.1016/j.compchemeng.2023.108367>. URL <https://www.sciencedirect.com/science/article/pii/S0098135423002375>.
- Carlos Andrés Elorza Casas, Luis A Ricardez-Sandoval, and Joshua L Pulsipher. A comparison of strategies to embed physics-informed neural networks in nonlinear model predictive control formulations solved via direct transcription. *arXiv preprint arXiv:2501.06335*, 2025.
- Xiangjun Huang, Kyriakos Kandris, and Evina Katsou. Training stiff neural ordinary differential equations in data-driven wastewater process modelling. *Journal of Environmental Management*, 373:123870, 2025. ISSN 0301-4797. doi: <https://doi.org/10.1016/j.jenvman.2024.123870>. URL <https://www.sciencedirect.com/science/article/pii/S030147972403857X>.
- Yicun Huang, Changfu Zou, Yang Li, and Torsten Wik. Minn: Learning the dynamics of differential-algebraic equations and application to battery modeling. *IEEE Transactions on Pattern Analysis and Machine Intelligence*, 2024.
- Tannan Xiao, Ying Chen, Shaowei Huang, Tirui He, and Huizhe Guan. Feasibility study of neural ode and dae modules for power system dynamic component modeling. *IEEE Transactions on Power Systems*, 38(3):2666–2678, 2022.
- William Bradley and Fani Boukouvala. Two-stage approach to parameter estimation of differential equations using neural odes. *Industrial & Engineering Chemistry Research*, 60(45):16330–16344, 2021. doi: 10.1021/acs.iecr.1c00552. URL <https://doi.org/10.1021/acs.iecr.1c00552>.
- Angan Mukherjee and Debangsu Bhattacharyya. Development of mass, energy, and thermodynamics constrained steady-state and dynamic neural networks for interconnected chemical systems. *Chemical Engineering Science*, page 121506, 2025.
- Vincenzo Di Vito, Mostafa Mohammadian, Kyri Baker, and Ferdinando Fioretto. Learning to solve differential equation constrained optimization problems. *arXiv preprint arXiv:2410.01786*, 2024.
- Christian Moya and Guang Lin. Dae-pinn: a physics-informed neural network model for simulating differential algebraic equations with application to power networks. *Neural Computing and Applications*, 35(5):3789–3804, 2023.
- Jiasheng Chen, Juan Tang, Ming Yan, Shuai Lai, Kun Liang, Jianguang Lu, and Wenqiang Yang. Physical information neural networks for solving high-index differential-algebraic equation systems based on radau methods. *arXiv preprint arXiv:2310.12846*, 2023.
- Kai Luo, Juan Tang, Mingchao Cai, Xiaoqing Zeng, Manqi Xie, and Ming Yan. Dae-kan: A kolmogorov-arnold network model for high-index differential-algebraic equations. *arXiv preprint arXiv:2504.15806*, 2025.

- Alistair White, Anna Büttner, Maximilian Gelbrecht, Valentin Duruisseaux, Niki Kilbertus, Frank Hellmann, and Niklas Boers. Projected neural differential equations for learning constrained dynamics. *arXiv preprint arXiv:2410.23667*, 2024.
- Avik Pal, Alan Edelman, and Christopher Rackauckas. Semi-explicit neural daes: Learning long-horizon dynamical systems with algebraic constraints. *arXiv preprint arXiv:2505.20515*, 2025.
- James Koch, Madelyn Shapiro, Himanshu Sharma, Draguna Vrabe, and Ján Drgoňa. Learning neural differential algebraic equations via operator splitting. In *2025 IEEE 64th Conference on Decision and Control (CDC)*, pages 2077–2084. IEEE, 2025.
- Aaron Tuor, Jan Drgona, and Draguna Vrabe. Constrained neural ordinary differential equations with stability guarantees. *arXiv preprint arXiv:2004.10883*, 2020.
- Cyrus Neary, Nathan Tsao, and Ufuk Topcu. Neural port-hamiltonian differential algebraic equations for compositional learning of electrical networks. *arXiv preprint arXiv:2412.11215*, 2024.
- Elisabeth Roesch, Christopher Rackauckas, and Michael PH Stumpf. Collocation based training of neural ordinary differential equations. *Statistical applications in genetics and molecular biology*, 20(2):37–49, 2021.
- Lorenz T. Biegler. An overview of simultaneous strategies for dynamic optimization. *Chemical Engineering and Processing: Process Intensification*, 46(11):1043–1053, 2007. ISSN 0255-2701. doi: <https://doi.org/10.1016/j.ccep.2006.06.021>. URL <https://www.sciencedirect.com/science/article/pii/S0255270107001122>. Special Issue on Process Optimization and Control in Chemical Engineering and Processing.
- Andreas Wächter and Lorenz T Biegler. On the implementation of an interior-point filter line-search algorithm for large-scale nonlinear programming. *Mathematical programming*, 106:25–57, 2006.
- John D. Hedengren, Reza Asgharzadeh Shishavan, Kody M. Powell, and Thomas F. Edgar. Nonlinear modeling, estimation and predictive control in APMonitor. *Computers & Chemical Engineering*, 70:133 – 148, 2014. ISSN 0098-1354. doi: 10.1016/j.compchemeng.2014.04.013.
- Joshua L Pulsipher, Weiqi Zhang, Tyler J Hongisto, and Victor M Zavala. A unifying modeling abstraction for infinite-dimensional optimization. *Computers & Chemical Engineering*, 156:107567, 2022.
- Bethany Nicholson, John D. Sirola, Jean-Paul Watson, Victor M. Zavala, and Lorenz T. Biegler. pyomo.dae: a modeling and automatic discretization framework for optimization with differential and algebraic equations. *Mathematical Programming Computation*, 10(2):187–223, 2018. doi: 10.1007/s12532-017-0127-0. URL <https://doi.org/10.1007/s12532-017-0127-0>.
- Mariia Shapovalova and Calvin Tsay. Training neural odes using fully discretized simultaneous optimization**support from a basf/royal academy of engineering senior research fellowship is gratefully acknowledged. *IFAC-PapersOnLine*, 59(6):469–474, 2025. ISSN 2405-8963. doi: <https://doi.org/10.1016/j.ifacol.2025.07.190>. URL <https://www.sciencedirect.com/science/article/pii/S2405896325005506>. 14th IFAC Symposium on Dynamics and Control of Process Systems, including Biosystems DYCOPS 2025.
- Lorenz T Biegler. *Nonlinear programming: concepts, algorithms, and applications to chemical processes*. SIAM, Philadelphia, PA, 2010.
- Uri M Ascher and Linda R Petzold. *Computer methods for ordinary differential equations and differential-algebraic equations*. SIAM, Philadelphia, PA, 1998.
- Robert Fourer, David M Gay, and Brian W Kernighan. A modeling language for mathematical programming. *Management Science*, 36(5):519–554, 1990.
- Iain S Duff and John K Reid. *MA27—a set of Fortran subroutines for solving sparse symmetric sets of linear equations*. UKAEA Atomic Energy Research Establishment, Harwell, UK, 1982.
- James Bradbury, Roy Frostig, Peter Hawkins, Matthew James Johnson, Chris Leary, Dougal Maclaurin, George Necula, Adam Paszke, Jake VanderPlas, Skye Wanderman-Milne, and Qiao Zhang. JAX: composable transformations of Python+NumPy programs, 2018. URL <http://github.com/google/jax>.
- Jorge Nocedal and Stephen J Wright. *Numerical optimization*. Springer, New York, NY, 1999.
- Robert B Parker, Oscar Dowson, Nicole LoGiudice, Manuel Garcia, and Russell Bent. Formulations and scalability of neural network surrogates in nonlinear optimization problems. *arXiv preprint arXiv:2412.11403*, 2024.
- Victor M Zavala, Carl D Laird, and Lorenz T Biegler. Interior-point decomposition approaches for parallel solution of large-scale nonlinear parameter estimation problems. *Chemical Engineering Science*, 63(19):4834–4845, 2008.
- Jia Kang, Yankai Cao, Daniel P Word, and Carl D Laird. An interior-point method for efficient solution of block-structured nlp problems using an implicit schur-complement decomposition. *Computers & Chemical Engineering*, 71:563–573, 2014.

- Laurens R Lueg, Michael L Bynum, Carl D Laird, and Lorenz T Biegler. Domain decomposition preconditioners for schur complement systems arising in structured nonlinear optimization problems: Lr lueg et al. *Optimization and Engineering*, pages 1–31, 2025.
- François Pacaud. Sensitivity analysis for parametric nonlinear programming: A tutorial. *arXiv preprint arXiv:2504.15851*, 2025.
- Hans Pirnay, Rodrigo López-Negrete, and Lorenz T Biegler. Optimal sensitivity based on ipopt. *Mathematical Programming Computation*, 4(4):307–331, 2012.
- Shawn T Brown, Paola Buitrago, Edward Hanna, Sergiu Sanielevici, Robin Scibek, and Nicholas A Nystrom. Bridges-2: A platform for rapidly-evolving and data intensive research. In *Practice and experience in advanced research computing 2021: Evolution across all dimensions*, pages 1–4. 2021.
- James Koch, Madelyn Shapiro, Himanshu Sharma, Draguna Vrabie, and Jan Drgona. Neural differential algebraic equations. *arXiv preprint arXiv:2403.12938*, 2024.
- Diederik P Kingma and Jimmy Ba. Adam: A method for stochastic optimization. *arXiv preprint arXiv:1412.6980*, 2014.
- Alexander D Bazykin. *Nonlinear dynamics of interacting populations*. World Scientific, Hackensack, NJ, 1998.
- Andrei Korobeinikov. A lyapunov function for leslie-gower predator-prey models. *Applied Mathematics Letters*, 14(6):697–700, 2001.
- Jeffrey Kantor. Fed-batch bioreactor (cbe30338 chemical process control notebook). <https://github.com/jckantor/CBE30338/blob/master/notebooks/02.07-Fed-Batch-Bioreactor.ipynb>, 2021. Course notebook, University of Notre Dame.
- Pauli Virtanen, Ralf Gommers, Travis E Oliphant, Matt Haberland, Tyler Reddy, David Cournapeau, Evgeni Burovski, Pearu Peterson, Warren Weckesser, Jonathan Bright, et al. Scipy 1.0: fundamental algorithms for scientific computing in python. *Nature methods*, 17(3):261–272, 2020.
- Lorenz T Biegler and David M Thierry. Large-scale optimization formulations and strategies for nonlinear model predictive control. *IFAC-PapersOnLine*, 51(20):1–15, 2018.
- Robert Parker, Oscar Dowson, Nicole LoGiudice, Manuel Garcia, and Russell Bent. Nonlinear optimization with gpu-accelerated neural network constraints. *arXiv preprint arXiv:2509.22462*, 2025.